Ultrasonics - Sonochemistry 49 (2018) 303–309

Contents lists available at ScienceDirect

Ultrasonics - Sonochemistry

journal homepage: www.elsevier.com/locate/ultson

Low intensity sonosynthesis of iron carbide@iron oxide core-shell nanoparticles

A.I. Argüelles-Pesqueira[a], N.M. Diéguez-Armenta[b], A.K. Bobadilla-Valencia[c], S.K. Nataraj[d], A. Rosas-Durazo[a], R. Esquivel[b], M.E. Alvarez-Ramos[b], R. Escudero[c], P. Guerrero-German[a], J.A. Lucero-Acuña[a,b], P. Zavala-Rivera[a,b,*]

[a] Posgrado en Ciencias de la Ingeniería, Departamento de Ingeniería Química y Metalurgia, Universidad de Sonora, 83000, Mexico
[b] Posgrado en Nanotecnología, Departamento de Física, Universidad de Sonora, 83000, Mexico
[c] Instituto de Investigaciones en Materiales, Universidad Nacional Autónoma de México, A.P. 70-360, Ciudad de México 04510, Mexico
[d] Centre for Nano and Material Sciences, Jain University, Jain Global Campus, Kanakapura, Ramanagaram, Bangalore 562112, India

A B S T R A C T

Here we demonstrate a simple method for the organic sonosynthesis of stable Iron Carbide@Iron Oxide core-shell nanoparticles (ICIONPs) stabilized by oleic acid surface modification. This robust synthesis route is based on the sonochemistry reaction of organometallic precursor like $Fe(CO)_5$ in octanol using low intensity ultrasonic bath. As obtained, nanoparticles diameter sizes were measured around 6.38 nm ± 1.34 with a hydrodynamic diameter around 25 nm and an estimated polydispersity of 0.27. Core-Shell structure of nanoparticles was confirmed using HR-TEM and XPS characterization tools in which a core made up of iron carbide (Fe_3C) and a shell of magnetite (γ-Fe_2O_3) was found. The overall nanoparticle presented ferromagnetic behavior at 4 K by SQUID. With these characteristics, the ICIONPs can be potentially used in various applications such as theranostic agent due to their properties obtained from the iron oxides and iron carbide phases.

1. Introduction

For several decades, metal and metal oxide nanoparticles (NPs) have been explored and utilized in a wide range of applications from catalysis, chemical sensors, nanocomposites, nanoelectronics [1,2] to biotechnology and nanomedicine [3]. Metal oxides are widely known metal-based materials due to their fascinating properties like magnetic momentum and chemical composition which allow them to tailor them to suffice versatility for different applications. In addition to this, metal-based nanoparticles can be prepared in relatively simple way in which their size, size distribution and shapes can be tuned to enhance material properties and therefore applications.

In the recent years, along with metal oxides [4] many researcher explored magnetic properties of metal alloys, borides [5–7] and carbides [8–11] which could be organic, air and/or aqueous stable. Among oxide materials, iron oxides nanoparticles (IONs) have been extensively used NPs due to their low-to-no toxicity and ability to show low magnetization under applied magnetic field conditions [12]. Previously, there were reported the synthesis of different nanosystems like polymeric vectors [13–15], metallic and IONs modified [4,16,17] used for medicine field as theranostic application which is described as both diagnosis device and therapeutic agents [4].

Furthermore, Iron carbide (IC) is known for its high magnetization properties and being extremely stable in air, however, it has been found difficult to prepare the IC in nano-architecture systems. Nevertheless, there are some reports showing the preparation of IC nanoparticles via laser ablation [18–20], explosions [21,22], pyrolysis of organometallic precursors [23,24] or hydrogels [2,25,26], and more recently based on sonochemistry couple with plasma [27]. However, all the methods have proven to be high cost preparation methods and yields low efficiency, uncontrolled particle size, high polydispersity range and large-scale growth of agglomerates resulting in poor overall properties. Researcher used ICs prepared by previously described methods as catalyst, composite in different nanosystems, MRI contrast agent and hyperthermia therapies [28] which show high magnetic saturation and chemical stability.

In this study, we report preparation of magnetic Iron Carbide@Iron Oxide core-shell nanoparticles (ICIONPs) with ferromagnetic properties. Also, due to their stability and magnetic properties, novel core-shell nanomaterials can be potential utilized in nanomedicine applications. Therefore, here we report a simple and cost effective method for the synthesis of well define spherical, monodispersed and ferromagnetic properties of iron carbide (Fe_3C) and iron oxide (γ-Fe_2O_3) core-shell nanoparticle using low intensity sonosynthesis route and organometallic precursors ($Fe(CO)_5$). As obtained nanoparticles have been extensively characterized using transmission electron microscopy

* Corresponding author at: Posgrado en Ciencias de la Ingeniería, Departamento de Ingeniería Química y Metalurgia, Universidad de Sonora, 83000, Mexico.
E-mail address: paul.zavala@unison.mx (P. Zavala-Rivera).

https://doi.org/10.1016/j.ultsonch.2018.08.017
Received 20 February 2018; Received in revised form 14 August 2018; Accepted 16 August 2018
Available online 17 August 2018
1350-4177/

(TEM), dynamic light scattering (DLS), Fourier transform IR spectroscopy (FTIR), x-ray photoelectron spectroscopy (XPS) and superconducting quantum interference device (SQUID).

2. Experimental

2.1. Reagents and materials

For the synthesis and purification of ICIONPs, iron pentacarbonyl ($Fe(CO)_5$), oleic acid (99%), 1-octanol (99%), absolute ethanol and toluene were purchase from Sigma-Aldrich (Merck) and used without further purification. For all washing purposes milli-Q ($18.2\,\mu\Omega^{-1}$) water was used.

2.2. Methods

The sonosynthesis was carried out using ultrasonic water-bath model Branson 3800 with a fabric frequency of 40 kHz. During sonication, 15 mL Falcon tubes were used and fill with at least 5 mL of solvent and keep submerge in the center of the bath. The temperature for most of the experiment was not controlled, because past experiments showed not effect among the 15–60 °C temperature range (See Supplementary Data, Fig. S1), although a maximum temperature around 50 °C was naturally and normally achieved inside the water bath during summer season experiments.

FTIR spectra were analyzed using KBr pellets or ATR diamond module (as specify) between the 4000 to 400 cm^{-1} on a Thermo Scientific iS50 Nicolet, Madison, WI, USA, equipment using a 2 cm^{-1} resolution and 64 scans per sample at room temperature (RT). Morphology and core-shell characteristic morphologies were confirmed by TEM (JEOL Jem2010F Field Emission) with a voltage of 200 keV on a 200-mesh carbon on copper grid (Ted Pella). The ICIONPs average diameter size and distribution was calculated by the digital images using ImageJ 1.51m9 software from Wayne Rasband, National Institute of Health; and the inter-planar distance was processed using Fast Fourier Transform by the same software [29]. Hydrodynamic diameter was measured with a Malvern Instrument Zetasizer Nano ZS at 37 °C. The XPS was measured on 1x1 cm glass substrate in a Perkin Elmer PH1 5100 with dual anode of Al/Mg, non-monochrome Mg radiation of 1253.6 eV. All the high-resolution spectra were adjusted to the C1 signal at 285 eV due to the oleic acid presence. Near spectra were adjust with a Gauss-Lorentz (70% Gauss) function and the background noise was eliminated by the Shirley method for the carbon and Tougaard method for O1s and $Fe2p_{3/2}$. Magnetic properties were obtained by SQUID using a MPMS-5S by Quantum Design at a temperature of 4 K and an intensity of the applied magnetic field ranging from −40 to 40 kOe.

2.3. Preparation of the ICIONPs.

Firstly, iron carbide@iron oxide nanoparticles were prepared as result of the reaction between iron pentacarbonyl and oxygen in ultrasonic bath. As prepared nanoparticles were showing propensity to agglomeration and were stabilized via surface modification. Hence, ICIONPs were modified to avoid agglomerations by particle-particle interaction, using oleic acid. The reaction starts with a solution with 1 mmol relation of $Fe(CO)_5$ and 3 mmol relation of oleic acid dissolved in 5 mL of 1-octanol used before in somewhere else [30,31]. The solution was placed in a 15 mL lid closed falcon tube located in the center of the ultrasonic bath filled with deionized water at room temperature for 40 min until turn color of the solution; open and close of the lid was done every 5 min to allow the atmospheric oxygen into the reaction and keeping it free of water splashes.

2.4. Purification of ICIONPs

The recovery of the ICIONPs from the residues and the polydispersity lowering was carried by the centrifugation at 7197*g* at RT of the sonosyntheses solution by the addition 3 mL of absolute alcohol for 20 min. This step was followed to remove the non-reacted precursors. The precipitate is re-suspended by the addition of a 13% v/v of oleic acid/toluene solution and centrifuged at the same conditions to remove the bigger particles. The solution was again re-precipitated following the first purification step mention herein to obtain the final product which could be dissolved in different solvents (toluene, benzene, dichloromethane, chloroform, tetrahydrofuran) as tried.

3. Results and discussions

3.1. Synthesis of ICIONPs

As mention before, the synthesis of iron carbide nanoparticles using iron pentacarbonyl has been possible by other groups with the use of high energy techniques, in which the chemical reaction usually described, involves the decarbolynation of the pentacarbonyl and the liberation of gaseous CO under inert atmosphere conditions [32]. Although, our method has showed the impossibility to form any kind of nanoparticle (characterized by TEM and DLS) achievable under inert atmosphere conditions (like Ar and N_2); actually, several experiments have been tried with the expectative of synthesize pure iron carbide nanoparticles without success, proof that there is the necessity of the modification of the atmosphere with constant atmospheric air or pure oxygen conditions.

Even, when the mechanism of the reaction is not the main purpose of this work, herein, we described the possible mechanism of synthesis of the ICIONPS coated with oleic acid. Here the reaction could happen in 3 possible steps: In the first step, the iron pentacarbonyl start a decarbolynation by the ultrasonic bath to produce Fe_3C nucleation points with the aid of the oxygen present in the tube, as shown in the Eq. (1); follow by its grow due to the formation of the hotspot by the cavitation (due to the lower vapor pressure of $Fe(CO)_5$ comparing it with the octanol). The second step described in the Eq. (2); follows the interaction of the iron carbide nanoparticle produced with the oxygen, leading to the formation of the iron oxide outer layer [33]. Finally, in the third step the oleic acid chains interact with the iron oxide surface by its carboxyl group forming a complex link as explained somewhere else [34], as shown in Fig. 1(a).

Preliminary results has showed that there is an effect in the yield and size of the ICIONPs related with the O_2 concentration, but the chemical mechanism, effect of the O_2 concentration and optimization of the reaction will be examined in future works by our group.

$$6Fe(CO)_5 + 13O_2 \xrightarrow{Sonication} 2Fe_3C + 28CO_2 \quad (1)$$

$$4Fe_3C + 13O_2 \xrightarrow{Sonication} 6Fe_2O_3 + 4CO_2 \quad (2)$$

3.2. Morphology characterization

The analysis of TEM shows a spherical morphology in which a contrast in the brightness between the nucleus and the shell of the ICIONP can be visualized, as shown in Fig. 1(b). It is interesting to notice that the iron oxide shell size was constant even when the iron carbide nucleus diameter varied; the length and thickness of the iron oxide layer was noted to be around 2.56 nm ± 0.4 (n = 157). However, smaller nanoparticles shows no signal of an iron carbide core [33]. These effects could be explained with hypothesis that the iron carbide core was formed first by the reaction showed in the Eq. (1) and the core keeps growing with the presence of oxygen and iron pentacarbonyl, aid by the energy delivered by the cavitation-implosion effect. The iron

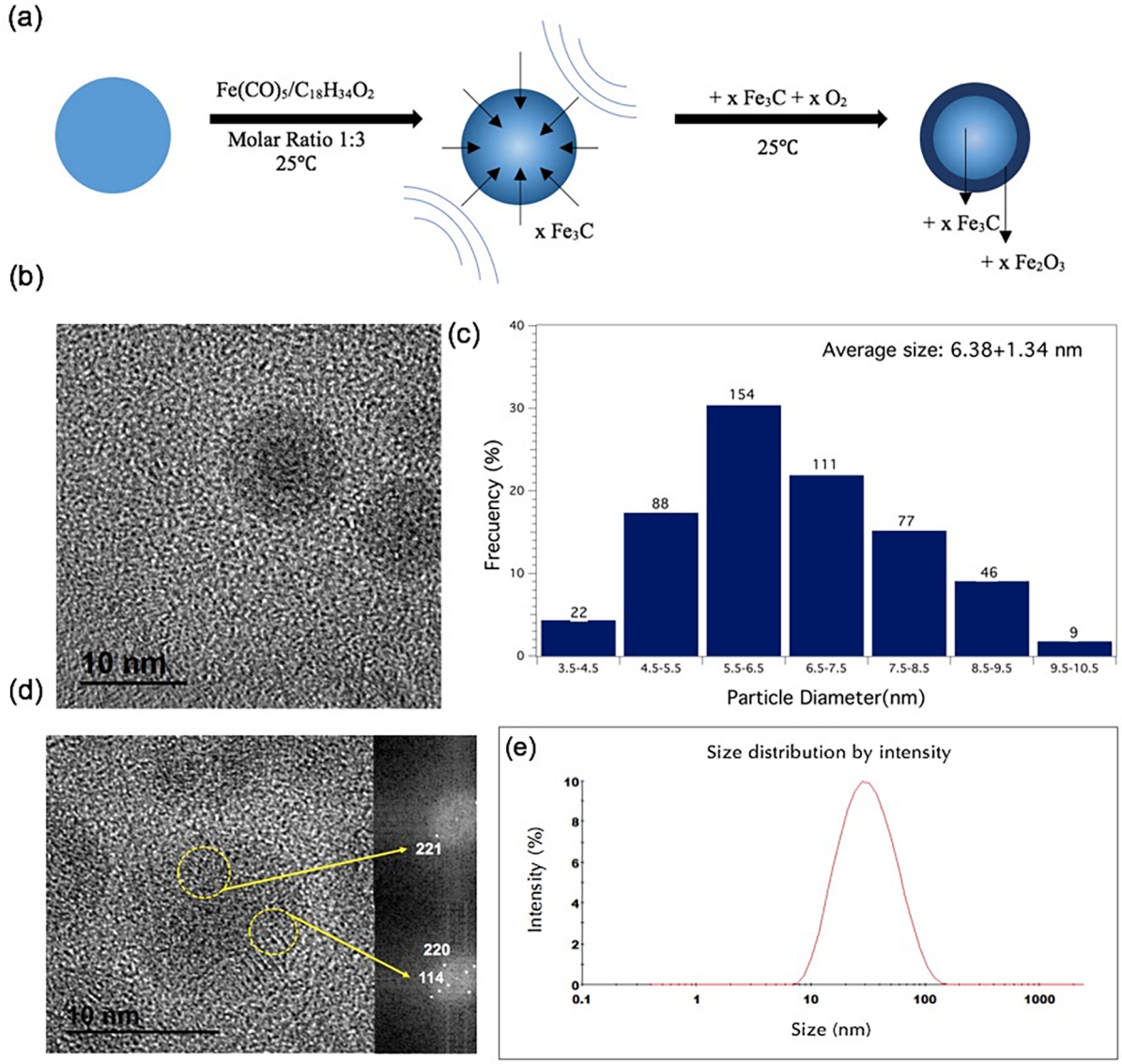

Fig. 1. Synthesis and characterization of ICIONPs (a) Sonosynthesis reaction leading to the formation of the ICIONPs coated with oleic acid. (b) TEM image of the ICIONPs coated with oleic acid, (c) Plot shows the nanoparticle size and their distribution, (d) HRTEM image showing the areas analyzed, area 1 being the core and area 2 for the shell of the ICION's. (e) DLS plot showing the ICIONPs intensity size distribution.

oxide is formed in the surface of the iron carbide by the oxidation induced again due to presence of dissolved oxygen. Other publications used high intensity sonication and inert atmospheres changing the reactions, probably, accelerating the oxidation of the seeded material and leading to the production of pure IONs. The nanoparticle diameters have been estimated from the TEM micrographs using the ImageJ 1.51 m9 software, the radius obtained was around 6.38 nm ± 1.34 (n = 509) as shown in the dispersion plot in Fig. 1(c). The HR-TEM analyzed on both, the area of the core and the shell were analyzed showing inter-planar distance of 2.10 Å (see Fig. 1(d)), typically to Cementite (Fe_3C) and the lattice inter-planar distance of 1.71 Å and 2.41 Å which corresponds to maghemite (γ-Fe_2O_3) phases. HR-TEM also shows an inter-planar distance of 4.29 Å and 2.88 Å which correspond a maghemite tetragonal super-cell and magnetite respectively [35,36]. Supplementary Data (Fig. S2) shows the EDS of the same samples with the elements expected for these reactions; like Fe, O and C. Also, the DLS results obtained at different concentrations of the disperse ICIONPs in toluene at 37 °C, showed a hydrodynamic diameter of 24.8 nm ± 3.73 (n = 16) and a polydispersity of 0.266 ± 0.0539, as shown in Fig. 1(e). The range of nanoparticle diameters can be explained by the presence of different amounts of oleic acid chains attached to the ICIONP surface and the stretch of the chains by the presence of the toluene, which is recognized as a good solvent for the oleic acid. Even though, the polydispersity obtained is in an adequate range expected for sonosynthesis reactions [37,38].

3.3. XPS results

Elemental composition of ICIONPs was confirmed by XPS analysis. The XPS spectra shown in Fig. 2(a), represents the principal elements found and list in the Table 1, identify with agreement of the literature [39]. On the other hand, Fig. 2(b), shows the photoelectronic peak, adjust to C 1S, in which the deconvolution showed three bands C—C, C—O or C═O and a third one corresponding to the Fe_3C [40]. Signals which agree with the results found for the inter-planar distance obtained by the HRTEM. It is important to mention that the energy values are shifted due to the adjustment from 287 to 285 eV made. Fig. 2(c), shows the adjust of the high-resolution peak of oxygen (O 1S) by the Toougard method presenting the band around 530.3 eV corresponding to the O-Fe of maghemita [40]. Iron characterization was more complicated; the oleic acid coating could be interfering with the signal. But

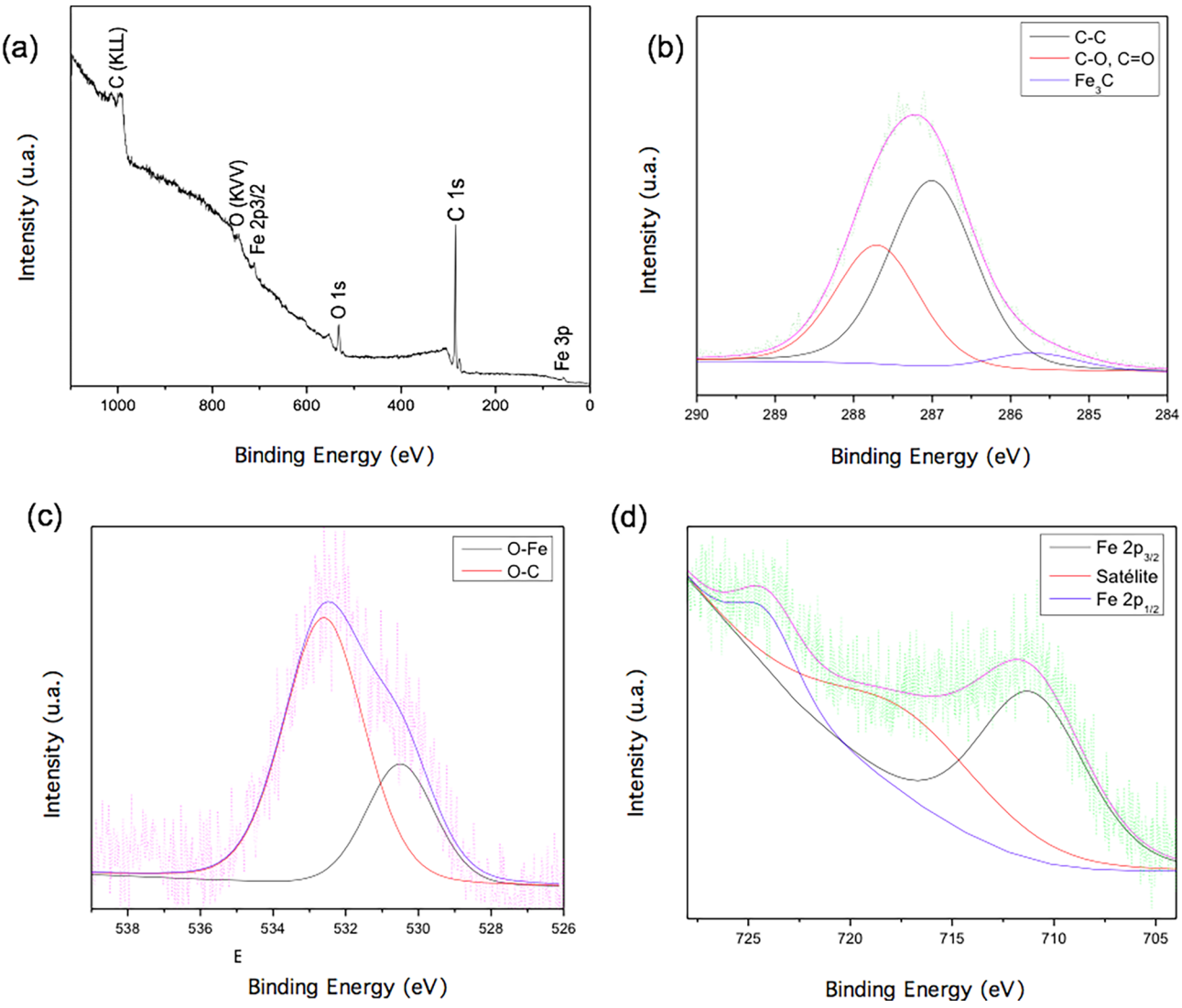

Fig. 2. XPS spectra of ICIONPs. (a) XPS survey spectra of the high-resolution peaks showing the principal elements found, (b) C 1S adjust showing the deconvolution of three different bands corresponding to C—C, C—O or C═O and Fe_3C. (c) O 1S adjusts showing the deconvolution of the O-C and O-Fe, being the later one like the maghemita signal. (d) Iron adjust signals deconvoluted showing the bands associated with $2p_{3/2}$and $2p_{1/2}$.

Table 1
Identify elements in ICIONPs sample.

Element	Position (eV)
C 1s	285
O 1s	533.2
Fe $2p_{3/2}$	711.7
Fe 3p	56.79

as the Fig. 2d showed the satellite $2p_{3/2}$ at 717.15 eV is appreciable. The band associate to Fe $2p_{1/2}$ is found around 711.1 eV, which is highly similar to maghemite report before [40]. Respect to the off-bending of the peak around 13 eV is explained by Fe $2p_{1/2}$.

3.4. FTIR characterization

FTIR characterization spectra recorded for ICIONPs in Fig. 3(a) illustrate the purification process of ICIONPs. The band at 1700 cm^{-1} after purification showing a reduction corresponding to the C═O of the carboxyl group and the appearance of the band at 1030 and 1050 cm^{-1} of the carboxylate (C—O) and the presence of carbon coated iron oxide with the 2920 cm^{-1} band [41].

3.5. Magnetic properties

The hysteresis loop measured at 4 K for the ICIONPs is shown in Fig. 4. As seen by the results, an atypical ferromagnetic behavior are showed if we compared this results with Fe_3O_4 nanoparticles synthesized with similar diameter sizes, usually showing superparamagnetic behavior [42]. The results showed a significant coercivity ($H_C \approx 2$ kOe), minimal remnant ($M_r \approx 0.07$ emu/g) and a relatively low saturation magnetization ($M_S \approx 0.78$ emu/g) given a remnant to saturation magnetization ratio: $M_r/M_S \approx 0.09$ (ICIONPs are coated with oleic acid increasing the amount of weight of nonmagnetic substance, hence reducing the overall magnetization of the material); these values has been usually presented as superparamagnetic behavior [28] and as ferrimagnetic by the presence of large particle (diameter ≈ 100 nm) below their blocking temperature by others [24,43], although this particles have demonstrated to be below the 10 nm diameter (according to the TEM data).

The probable explanation to a ferromagnetic behavior was approached by Borysiuk et al. [43]; in their work they synthesized Fe-C nanoparticles of similar sizes (10–100 nm) and proposed that the magnetic property is not attributed exclusively by the different fractions of magnetic material (iron carbide, iron oxide and oleic acid) but

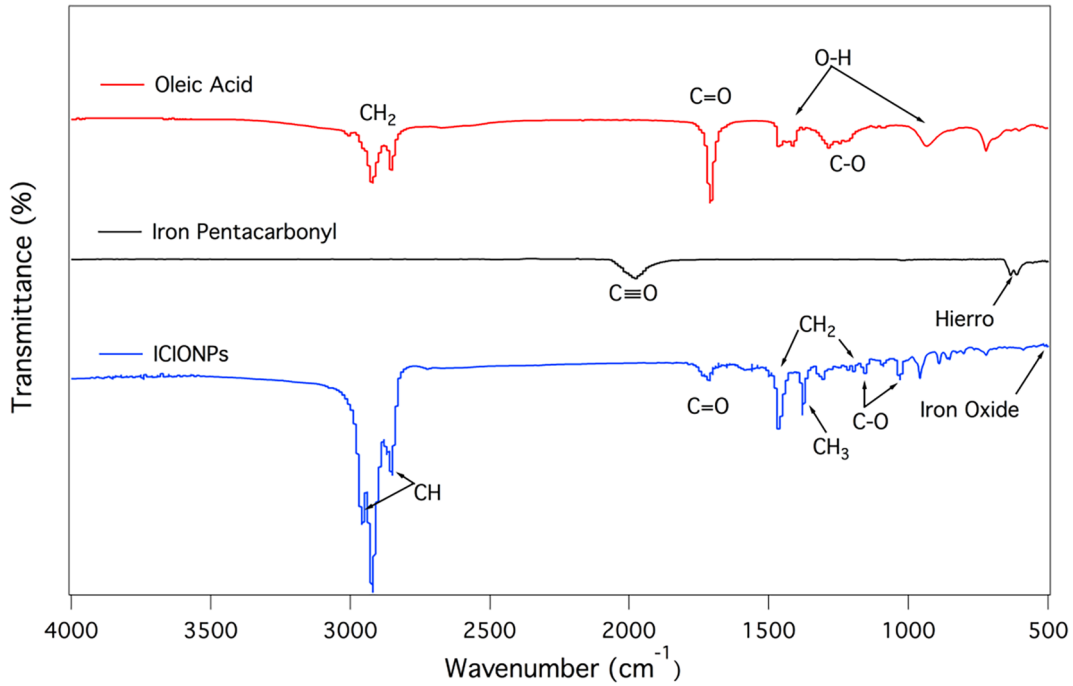

Fig. 3. FTIR characterization of ICIONPs. FTIR samples of the iron pentacarbonyl, oleic acid and the ICIONPs coated with oleic acid.

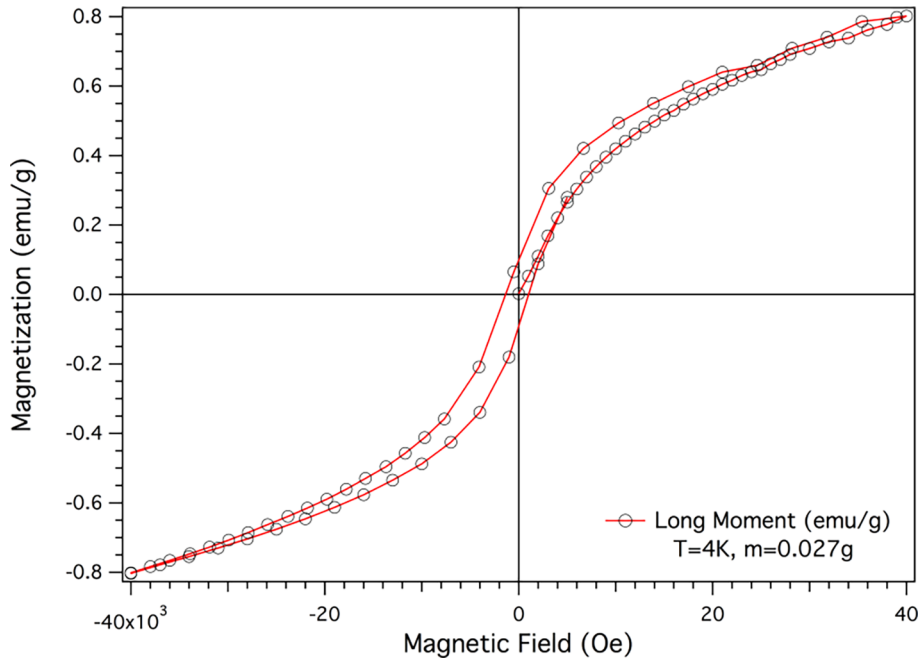

Fig. 4. Hysteresis loop of magnetization vs. applied magnetic field for ICIONPs at 4 K.

the weaker interaction between magnetic domains of the phases, as well to the nanoparticle size which could be bigger than the domain wall.

4. Conclusions

In this work, iron carbide@iron oxide core-shell nanoparticles stabilized with oleic acid were synthesized by low intensity sonication using a standard sonic water bath at room temperature. The diameter of the particles measured using HR-TEM noted to be around 6.38 nm with a visible core-shell architecture and a constant outer shell length of 2.5 nm. The diffraction spectra of the HR-TEM showed different interplanar distances between the core and the shell corresponding to iron carbide (Fe_3C) and iron oxide (γ-Fe_2O_3). These were corroborated by FTIR and XPS showing similar signals for those phases. Hydrodynamic diameter was measured by DLS using toluene dispersion at 37 °C obtaining sizes around 25 nm and low polydispersities of 0.266. Their magnetic properties were measured by SQUID at 4 K showing an unusual ferromagnetic behavior possible explained by the interaction of weaker magnetic moments and size domain wall due to the different core-shell phases which composed the nanoparticle, opening the possibility of being use as theranostic agent if the biocompatibility properties are achieved. Its development was only possible due to the use of low intensity ultrasonic equipment, opening the possibility to be

prepared in a simple, robust and cost-effective way without the need of sophisticated equipment.

Acknowledgements

P. Z-R is grateful with the “Secretaria de Educación Publica” SEP, Mexico; for the financial support through the NPTC program UNISON-PTC-250 of this work as well as sincerely appreciate the significant contributions made by Dr. Eduardo Larios-Rodríguez in the TEM characterization of the samples and with Dr. Josefina Alvaro-Rivera with the XPS interpretation. R. E. is grateful with DGAPA (UNAM), project IT100217. Finally, all the authors are grateful to “Consejo Nacional de Ciencia y Tecnología” CONACyT for the financial support through its different financial programs and scholarships.

Appendix A. Supplementary data

Supplementary data associated with this article can be found, in the online version, at https://doi.org/10.1016/j.ultsonch.2018.08.017.

References

[1] A. Ali, H. Zafar, M. Zia, I. ul Haq, A.R. Phull, J.S. Ali, et al., Synthesis, characterization, applications, and challenges of iron oxide nanoparticles, Nanotechnol. Sci. Appl. 9 (2016) 49–67, https://doi.org/10.2147/NSA.S99986.

[2] H. Wang, Z. Xu, H. Yi, H. Wei, Z. Guo, X. Wang, One-step preparation of single-crystalline Fe2O3 particles/graphene composite hydrogels as high performance anode materials for supercapacitors, Nano Energy 7 (2014) 86–96, https://doi.org/10.1016/J.NANOEN.2014.04.009.

[3] A.K. Gupta, M. Gupta, Synthesis and surface engineering of iron oxide nanoparticles for biomedical applications, Biomaterials 26 (2005) 3995–4021, https://doi.org/10.1016/j.biomaterials.2004.10.012.

[4] N. Lee, D. Yoo, D. Ling, M.H. Cho, T. Hyeon, J. Cheon, Iron oxide based nanoparticles for multimodal imaging and magnetoresponsive therapy, Chem. Rev. 115 (2015) 10637–10689, https://doi.org/10.1021/acs.chemrev.5b00112.

[5] M.A. Hamayun, M. Abramchuk, H. Alnasir, M. Khan, C. Pak, S. Lenhert, et al., Magnetic and magnetothermal studies of iron boride (FeB) nanoparticles, J. Magn. Magn. Mater. 451 (2018) 407–413, https://doi.org/10.1016/J.JMMM.2017.11.088.

[6] F. Wu, T. Li, X.R. Yang, C.M. Li, M.Q. Fan, K. Shu, Catalytic activity of cobalt boride nanoparticles on mobil crystalline material 41 for hydrogen, Instrum. Sci. Technol. 44 (2016) 425–434, https://doi.org/10.1080/10739149.2016.1142998.

[7] A.M. Keszler, P. Fazekas, E. Bódis, E. Drotár, S. Klébert, M. Boselli, et al., Optical emission spectroscopic study of the synthesis of titanium boride nanoparticles in RF thermal plasma reactor, Plasma Chem. Plasma Process. 37 (2017) 1491–1503, https://doi.org/10.1007/s11090-017-9836-4.

[8] J. Yu, F. Chen, W. Gao, Y. Ju, X. Chu, S. Che, et al., Iron carbide nanoparticles: an innovative nanoplatform for biomedical applications, Nanoscale Horizons 2 (2017) 81–88, https://doi.org/10.1039/C6NH00173D.

[9] Z. Yang, T. Zhao, X. Huang, X. Chu, T. Tang, Y. Ju, et al., Modulating the phases of iron carbide nanoparticles: from a perspective of interfering with the carbon penetration of Fe@Fe_3O_4 by selectively adsorbed halide ions, Chem. Sci. 8 (2017) 473–481, https://doi.org/10.1039/C6SC01819J.

[10] A. Bordet, L.-M. Lacroix, P.-F. Fazzini, J. Carrey, K. Soulantica, B. Chaudret, Magnetically induced continuous CO_2 hydrogenation using composite iron carbide nanoparticles of exceptionally high heating power, Angew. Chem. 128 (2016) 16126–16130, https://doi.org/10.1002/ange.201609477.

[11] X. Yang, X. Feng, H. Tan, H. Zang, X. Wang, Y. Wang, et al., N-Doped graphene-coated molybdenum carbide nanoparticles as highly efficient electrocatalysts for the hydrogen evolution reaction, J. Mater. Chem. A 4 (2016) 3947–3954, https://doi.org/10.1039/C5TA09507G.

[12] Y. Hou, Z. Xu, S. Sun, Controlled synthesis and chemical conversions of FeO nanoparticles, Angew. Chemie Int. Ed. 46 (2007) 6329–6332, https://doi.org/10.1002/anie.200701694.

[13] K. Zhu, Z. Deng, G. Liu, J. Hu, S. Liu, Photoregulated Cross-Linking of Superparamagnetic Iron Oxide Nanoparticle (SPION) loaded hybrid nanovectors with synergistic drug release and Magnetic Resonance (MR) imaging enhancement, Macromolecules 50 (2017) 1113–1125, https://doi.org/10.1021/acs.macromol.6b02162.

[14] D. Šmejkalová, K. Nešporová, G. Huerta-Angeles, J. Syrovátka, D. Jirák, A. Gálisová, et al., Selective in vitro anticancer effect of superparamagnetic iron oxide nanoparticles loaded in hyaluronan polymeric micelles, Biomacromolecules 15 (2014) 4012–4020, https://doi.org/10.1021/bm501065q.

[15] S. Laurent, D. Forge, M. Port, A. Roch, C. Robic, L. Vander Elst, et al., Magnetic iron oxide nanoparticles: synthesis, stabilization, vectorization, physicochemical characterizations, and biological applications, Chem. Rev. 108 (2008) 2064–2110, https://doi.org/10.1021/cr068445e.

[16] D. Alcantara, S. Lopez, M.L. García-Martin, D. Pozo, Iron oxide nanoparticles as magnetic relaxation switching (MRSw) sensors: current applications in nanomedicine, Nanomedicine Nanotechnology, Biol. Med. 12 (2016) 1253–1262, https://doi.org/10.1016/J.NANO.2016.01.005.

[17] K. Chatterjee, S. Sarkar, K. Jagajjanani Rao, S. Paria, Core/shell nanoparticles in biomedical applications, Adv. Colloid Interface Sci. 209 (2014) 8–39, https://doi.org/10.1016/J.CIS.2013.12.008.

[18] T. Matsue, Y. Yamada, Y. Kobayashi, Iron carbide nanoparticles produced by laser ablation in organic solvent, ICAME 2011, Springer, Netherlands, Dordrecht, 2013, pp. 179–183, , https://doi.org/10.1007/978-94-007-4762-3_27.

[19] P. Maneeratanasarn, T. Van Khai, S.Y. Kim, B.G. Choi, K.B. Shim, Synthesis of phase-controlled iron oxide nanoparticles by pulsed laser ablation in different liquid media, Phys. Status Solidi 210 (2013) 563–569, https://doi.org/10.1002/pssa.201228427.

[20] V. Amendola, P. Riello, M. Meneghetti, Magnetic nanoparticles of iron carbide, iron oxide, iron@iron oxide, and metal iron synthesized by laser ablation in organic solvents, J. Phys. Chem. C 115 (2011) 5140–5146, https://doi.org/10.1021/jp109371m.

[21] J. Kang, Y. Kim, H.-M. Kim, X. Hu, N. Saito, J.-H. Choi, et al., In-situ one-step synthesis of carbon-encapsulated naked magnetic metal nanoparticles conducted without additional reductants and agents, Sci. Rep. 6 (2016) 38652, https://doi.org/10.1038/srep38652.

[22] W. Wu, Z. Zhu, Z. Liu, Y. Xie, J. Zhang, T. Hu, Preparation of carbon-encapsulated iron carbide nanoparticles by an explosion method, Carbon N. Y. 41 (2003) 317–321, https://doi.org/10.1016/S0008-6223(02)00292-0.

[23] H. Huang, X. Feng, C. Du, S. Wu, W. Song, One-step pyrolytic synthesis of small iron carbide nanoparticles/3D porous nitrogen-rich graphene for efficient electrocatalysis, J. Mater. Chem. A 3 (2015) 4976–4982, https://doi.org/10.1039/C4TA06742H.

[24] G. Schinteie, V. Kuncser, P. Palade, F. Dumitrache, R. Alexandrescu, I. Morjan, et al., Magnetic properties of iron–carbon nanocomposites obtained by laser pyrolysis in specific configurations, J. Alloys Compd. 564 (2013) 27–34, https://doi.org/10.1016/J.JALLCOM.2013.02.126.

[25] H. Liu, C. Wang, Q. Gao, X. Liu, Z. Tong, Magnetic hydrogels with supracolloidal structures prepared by suspension polymerization stabilized by Fe2O3 nanoparticles, Acta Biomater. 6 (2010) 275–281, https://doi.org/10.1016/J.ACTBIO.2009.06.018.

[26] N.S. Satarkar, D. Biswal, J.Z. Hilt, Hydrogel nanocomposites: a review of applications as remote controlled biomaterials, Soft Matter 6 (2010) 2364, https://doi.org/10.1039/b925218p.

[27] R. Sergiienko, E. Shibata, Z. Akase, H. Suwa, T. Nakamura, D. Shindo, Carbon encapsulated iron carbide nanoparticles synthesized in ethanol by an electric plasma discharge in an ultrasonic cavitation field, Mater. Chem. Phys. 98 (2006) 34–38, https://doi.org/10.1016/j.matchemphys.2005.08.064.

[28] R.M. Patil, P.B. Shete, N.D. Thorat, S.V. Otari, K.C. Barick, A. Prasad, et al., Non-aqueous to aqueous phase transfer of oleic acid coated iron oxide nanoparticles for hyperthermia application, RSC Adv. 4 (2014) 4515–4522, https://doi.org/10.1039/C3RA44644A.

[29] C. Igathinathane, L.O. Pordesimo, E.P. Columbus, W.D. Batchelor, S.R. Methuku, Shape identification and particles size distribution from basic shape parameters using ImageJ, Comput. Electron. Agric. 63 (2008) 168–182, https://doi.org/10.1016/J.COMPAG.2008.02.007.

[30] R.A. Pérez, B. Albero, J.L. Tadeo, C. Sánchez-Brunete, Oleate functionalized magnetic nanoparticles as sorbent for the analysis of polychlorinated biphenyls in juices, Microchim. Acta. 183 (2016) 157–165, https://doi.org/10.1007/s00604-015-1617-2.

[31] D. Cho, J.-H. Baik, D. Choi, C.S. Lee, Dispersion stability of 1-octanethiol coated Cu nanoparticles in a 1-octanol solvent for the application of nanoink, Appl. Surf. Sci. 309 (2014) 300–305, https://doi.org/10.1016/J.APSUSC.2014.04.203.

[32] I. Morjan, F. Dumitrache, R. Alexandrescu, C. Fleaca, R. Birjega, C.R. Luculescu, et al., Laser synthesis of magnetic iron–carbon nanocomposites with size dependent properties, Adv. Powder Technol. 23 (2012) 88–96, https://doi.org/10.1016/J.APT.2010.12.014.

[33] H. Khurshid, C.G. Hadjipanayis, H. Chen, W. Li, H. Mao, R. Machaidze, et al., Core/shell structured iron/iron-oxide nanoparticles as excellent MRI contrast enhancement agents, J. Magn. Magn. Mater. 331 (2013) 17–20, https://doi.org/10.1016/J.JMMM.2012.10.049.

[34] M. Bloemen, W. Brullot, T.T. Luong, N. Geukens, A. Gils, T. Verbiest, Improved functionalization of oleic acid-coated iron oxide nanoparticles for biomedical applications, J. Nanoparticle Res. 14 (2012) 1100, https://doi.org/10.1007/s11051-012-1100-5.

[35] R.A. Bepari, P. Bharali, B.K. Das, Controlled synthesis of α- and γ-Fe2O3 nanoparticles via thermolysis of PVA gels and studies on α-Fe2O3 catalyzed styrene epoxidation, J. Saudi Chem. Soc. 21 (2017) S170–S178, https://doi.org/10.1016/J.JSCS.2013.12.010.

[36] W. Cheng, K. Tang, Y. Qi, J. Sheng, Z. Liu, One-step synthesis of superparamagnetic monodisperse porous Fe3O4 hollow and core-shell spheres, J. Mater. Chem. 20 (2010) 1799, https://doi.org/10.1039/b919164j.

[37] X. Teng, H. Yang, Effects of surfactants and synthetic conditions on the sizes and self-assembly of monodisperse iron oxide nanoparticlesElectronic supplementary information (ESI) available: XRD data of iron oxide nanoparticles, Fig. S1 and S2. See http://www.rsc.org/suppd, J. Mater. Chem. 14 (2004) 774, https://doi.org/10.1039/b311610g.

[38] W. Wu, Q. He, C. Jiang, Magnetic iron oxide nanoparticles: synthesis and surface functionalization strategies, Nanoscale Res. Lett. 3 (2008) 397–415, https://doi.org/10.1007/s11671-008-9174-9.

[39] D. Briggs, Handbook of X-ray Photoelectron Spectroscopy C. D. Wanger, W. M. Riggs, L. E. Davis, J. F. Moulder and G. E.Muilenberg Perkin-Elmer Corp., Physical

Electronics Division, Eden Prairie, Minnesota, USA, 1979. 190 pp. $195, Surf. Interface Anal. 3 (1981) v–v. doi:10.1002/sia.740030412.
[40] A.V. Naumkin, A. Kraut-Vass, S.W. Gaarenstroom, C.J. Powell, NIST X-ray Photoelectron Spectroscopy (XPS) Database, Version 3, (2012).
[41] H. Bae, T. Ahmad, I. Rhee, Y. Chang, S.-U. Jin, S. Hong, Carbon-coated iron oxide nanoparticles as contrast agents in magnetic resonance imaging, Nanoscale Res. Lett. 7 (2012) 44, https://doi.org/10.1186/1556-276X-7-44.
[42] D.K. Kim, Y. Zhang, W. Voit, K.V. Rao, M. Muhammed, Synthesis and characterization of surfactant-coated superparamagnetic monodispersed iron oxide nanoparticles, J. Magn. Magn. Mater. 225 (2001) 30–36, https://doi.org/10.1016/S0304-8853(00)01224-5.
[43] J. Borysiuk, A. Grabias, J. Szczytko, M. Bystrzejewski, A. Twardowski, H. Lange, Structure and magnetic properties of carbon encapsulated Fe nanoparticles obtained by arc plasma and combustion synthesis, Carbon N. Y. 46 (2008) 1693–1701, https://doi.org/10.1016/J.CARBON.2008.07.011.